J. Fluid Mech. (1989), *vol.* 198, *pp.* 293–319
Printed in Great Britain

Phase changes following the initiation of a hot turbulent flow over a cold solid surface

By HERBERT E. HUPPERT

Department of Applied Mathematics and Theoretical Physics, University of Cambridge, Silver Street, Cambridge CB3 9EW, U.K.

(Received 15 March 1988)

We analyse the melting and/or freezing that can occur when a very large layer of hot fluid begins to flow turbulently over a cold solid retaining boundary. This is a form of Stefan problem and the response is determined by the balance between the turbulent heat flux from the fluid, H, and the (initially infinite) conductive flux into the solid. We show that solidification of the flow at the boundary must always occur initially, unless the freezing temperature of the fluid, T_f, is less than the initially uniform temperature, T_0, of the semi-infinite solid. We determine the evolution of the solidified region and show that with time it will be totally remelted. Melting and ablation of the solid retaining boundary will then generally follow, unless its melting temperature exceeds that of the turbulent flow. The maximum thickness of the solidified crust is shown to scale with $k^2(T_f-T_0)^2/\rho\kappa HL$ and its evolution takes place on a timescale of $k^2(T_f-T_0)^2/\kappa H^2$, where k is the thermal conductivity, κ the thermal diffusivity, ρ the density and L the latent heat, with all these material properties assumed to be equal for fluid and solid.

1. Introduction

On many a cold winter's morning hot water is thrown out over hard snow and ice. The aim is for the thermal energy in the hot water to melt some (if not all) of the ice and snow. Alternatively, however, the hot water may freeze without melting the ice. What are the conditions that distinguish the freezing of hot fluid from the melting of cold solid?

Another motivation for this paper arises from the study of the flow of hot turbulent lava over relatively cold solid ground. This occurred frequently during the Archaen age from 4.0 to 2.5×10^9 years ago. At that time, some erupted lavas were as much as 400 °C hotter than those of today. Their magnesium oxide content was also considerably greater than that of present-day lavas. Owing to these two facts, the viscosity of Archaen lavas (c. 1 $\mathrm{cm^2\,s^{-1}}$) was considerably less than that of modern lavas (> 100 $\mathrm{cm^2\,s^{-1}}$). Huppert *et al.* (1984) demonstrated that because of this relatively low viscosity, Archaen lava flows would have been turbulent (in contrast to the generally laminar lava flows of today). They argued that the hot turbulent flows would have been able to transfer their heat to the ground sufficiently rapidly to melt the base rock over which they flowed and form thermal erosion channels. Huppert *et al.* (1984) and Huppert & Sparks (1985) (reviewed in Huppert 1986) calculated the rate of melting of the bed rock using a quasi steady-state model, which they argued would be valid some time after the initiation of the flow. There was some debate about their approach, with a number of geoscientists suggesting that the lava flow might continuously solidify from its base and not melt the bed rock

at all (see, for example, Claoué-Long & Nesbitt 1985). An aim of this paper is to provide a quantitative evaluation of this suggestion; and to show it to be incorrect when applied to a thick turbulent lava flow.

The paper achieves considerably more than this aim, however, by investigating the phase changes that can occur in a situation that is a variant of the familiar Stefan problem in quite some generality.

We assume that a turbulent flow is initiated over a cold solid and that the downward heat transfer is a given function of the difference in temperatures in the main body of the turbulent fluid and at the fluid/solid interface. For simplicity, we shall assume that the turbulent flow is very thick and thus maintains its temperature as it flows over the ground. The basic ideas could be incorporated into a time-dependent model which allowed the turbulent flow to change gradually, but this goes beyond the aim of the present calculations. For our purposes, it suffices that the change in thickness of the flow due to any solidification or melting be small. The assumption that the forward velocity of the turbulent flow along the ground greatly exceeds that of the thermal diffusion front indicates that only the vertical propagation of heat needs to be considered. We also assume that the heat flux from the turbulent flow responds instantaneously to the temperature at its boundary. This requires that the timescale of the turbulent flow and its adjustment be much less than the timescale of the solidification and/or melting, as calculated below.

The situation is then completely specified by the functional dependence of the heat flux from the turbulent flow to the solid, its latent heat and thermal diffusivity (which are assumed to be equal to those of the fluid) and four temperatures: that of the main body of the turbulent fluid, say T_∞; the initial temperature of the solid, say T_0; the freezing temperature of the fluid, say T_f, which by hypothesis is less than T_∞; and the melting temperature of the solid, say T_m, which by hypothesis exceeds T_0. The simplest case to analyse, which illustrates the most important of the new effects, occurs when the temperatures of melting and freezing are identical; that is when $(T_0 <) T_m = T_f (< T_\infty)$. We concentrate on this case in §2. In §§3 and 4 we evaluate the response for $T_f < T_m$ and in §5 that when $T_f > T_m$.

While there are four temperatures which need to be specified, only the differences between three of these temperatures and the fourth are relevant. From these three temperature differences, two non-dimensional quantities which describe the system can be obtained. We find it convenient to define these as

$$\alpha = \frac{T_\infty - T_m}{T_m - T_0}, \quad \beta = \frac{T_\infty - T_m}{T_\infty - T_f}, \tag{1.1a, b}$$

where α and β must be of the same sign because $T_f < T_\infty$ and $T_0 < T_m$. These inequalities also restrict α and β further, and only a minor part of the (α, β)-plane need be investigated.

The main result, which is highlighted in §2 and sketched in figure 1, is that the turbulent flow must initially freeze against the cold solid boundary and form what is called by geologists a chilled margin. With time the chill in the situation considered here must melt back and melting of the original solid can follow. Except when $T_f \leqslant T_0$, the initial formation and subsequent melting of the chill always occurs. The underlying solid will then melt unless $T_\infty \leqslant T_m$. Additional effects can also occur, such as the elapse of some time between the melting back of the chilled margin and commencement of melting of the original solid, or the initiation of melting of the original solid before the chill has totally melted. These situations arise and are analysed in §§4 and 5.

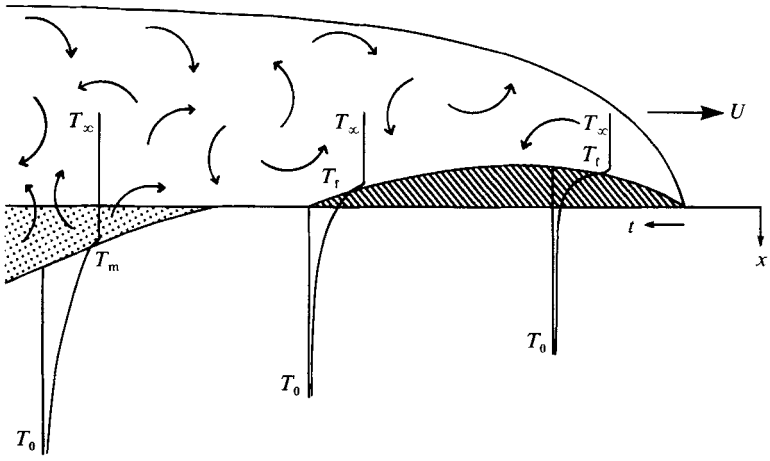

FIGURE 1. A sketch, with considerable vertical exaggeration, of the flow configuration and temperature profiles. The hot turbulent current, designated as ⟳, moves forward with speed U to initiate the heat transfer to the ground and promote freezing or melting, designated by ▨ and ⁘ respectively. We assume that the horizontal lengthscale of change, l_H, greatly exceeds the vertical scale, l_V, and so horizontal diffusion of the temperature profile can be neglected. The response at any fixed horizontal coordinate is then a function only of the vertical coordinate x and time t, defined as shown. The displayed temperatures T_0, T_m, T_f and T_∞ are defined in the text.

Mathematically, the problem under consideration is a variant of the classical Stefan problem, which has a long history (see, for example, Hill 1987 and Tarzia 1988). The situation analysed here is dominated by the initial discontinuity in temperature at the solid boundary and the subsequent non-monotonic response of the boundary. The formation of a chill means that the region occupied by solid, in which the heat conduction equation needs be solved, increases with time. The incorporation of this new region through the boundary and its subsequent expulsion, can give rise to certain analytical difficulties, as discussed in Appendix C. To my knowledge such a situation has only arisen once previously, in the quite different problem analysed by Crowley & Ockendon (1977). Geologically, the melting back of a chilled margin is a new idea, and to my knowledge has only appeared before in the work of my research student P. M. Bruce (1989), who has analysed the continuing laminar flow up a vertical, smooth-walled dyke. He showed that the flow first freezes, to form a chill against the wall, but that the thermal energy continually supplied by the flow could, under criteria he calculated, melt back the chill. The timescale in this laminar situation is very much longer than that calculated for the present turbulent flow.

2. Equal melting and freezing temperatures

We commence this section with a physical description of the response, which will help to explain the subsequent mathematical development. Initially, the temperature in the turbulent fluid is uniformly T_∞ and that in the solid T_0, with $T_m = T_f$ lying between these, as sketched in figure 2. Instantaneously, the temperature profile must become continuous across the solid/fluid interface. Denote the temperature at the (moving) interface by T_i. The turbulent flow adjusts on a very short timescale

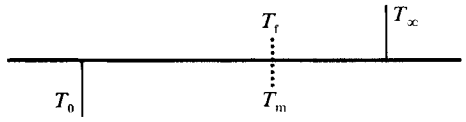

FIGURE 2. A sketch of the distribution of temperatures with $T_0 < T_m = T_f < T_\infty$.

(infinitesimally short by our already stated assumptions) to have a thin thermal boundary layer at the base of which there is a heat flux

$$H = f(T_\infty - T_i), \tag{2.1}$$

where f is some continuous, positive function of its positive argument. At $t = 0+$ the interfacial temperature T_i cannot exceed T_f because this would imply that part of the solid had melted instantaneously. Similarly, T_i cannot be less than T_f because this would imply that the base of the turbulent flow had solidified instantaneously. Thus $T_i = T_f$ initially. As the boundary between fluid and solid evolves, T_i will continue to equal T_f.

The finite heat flux into the interface, H, occurs simultaneously with a large (initially infinitely large) conductive heat flux in the solid away from the interface, say F. The fluxes H and F can only be balanced by the latent-heat release provided by solidification of the base of the turbulent flow. We thus argue that solidification of the fluid must be the first response (initially at an infinite rate). As time proceeds, however, F decreases monotonically as the conductive temperature profile relaxes. There will thus come a time when H first exceeds F and subsequently melting at the interface occurs. The previously solidified layer will melt first, followed by the semi-infinite, solid half-space.

We now present the quantitative analysis. Consider the fixed flux H to be incident on the fluid/solid interface at $x = a(t)$, where x is the coordinate axis with $x > 0$ specifying the original solid half-space. Denote by $T(x, t)$ the conductive temperature profile in the solid. The governing equations then are

$$T_t = \kappa T_{xx} \quad (x > a(t)), \tag{2.2}$$

$$T = T_f, \quad \rho L\dot{a} = H + kT_x \quad (x = a(t)), \tag{2.3a, b}$$

$$T \to T_0 \quad (x \to \infty), \tag{2.4}$$

$$T = T_0 \quad (t = 0, \quad x > 0), \tag{2.5}$$

where ρ and L are the density and latent heat, which for simplicity we shall assume identical for both the fluid and the solid, κ is the thermal diffusivity and k is the thermal conductivity.

It is convenient to introduce non-dimensional variables into (2.2)–(2.5) by writing

$$T = T_0 + (T_f - T_0)\,\theta, \tag{2.6a}$$

$$x = k(T_f - T_0)\,\xi/H, \tag{2.6b}$$

$$t = \tfrac{1}{4}k^2(T_f - T_0)^2\tau/\kappa H^2 \tag{2.6c}$$

and

$$a = k(T_f - T_0)\,\eta/H. \tag{2.6d}$$

The system can then be described in terms of one parameter, the Stefan number

$$S = L/[c(T_f - T_0)], \tag{2.7}$$

where c is the specific heat of both fluid and solid, as

$$\theta_\tau = \tfrac{1}{4}\theta_{\xi\xi} \quad (\xi > \eta(\tau)), \tag{2.8}$$

$$\theta = 1, \quad 4S\dot{\eta} = 1 + \theta_\xi \quad (\xi = \eta(\tau)), \tag{2.9a, b}$$

$$\theta \to 0 \quad (\xi \to \infty), \tag{2.10}$$

$$\theta = 0 \quad (\tau = 0, \quad \xi > 0). \tag{2.11}$$

Physically, the Stefan number represents the ratio of the latent heat of melting to the heat needed to raise the solid from its initial temperature to its melting temperature.

The system (2.8)–(2.11) is nonlinear only through the application of (2.9) at the unknown, moving boundary $\eta(\tau)$. It is instructive to evaluate the solution of the derived linear problem that is obtained by applying (2.9) at $\xi = 0$ and determining η from (2.9*b*). This procedure leads directly to

$$\theta(\xi, \tau) = \operatorname{erfc}(\xi \tau^{-\frac{1}{2}}) \tag{2.12}$$

and

$$\eta(\tau) = \left[\tfrac{1}{4}\tau - \left(\frac{\tau}{\pi}\right)^{\frac{1}{2}}\right] S^{-1}. \tag{2.13}$$

Equation (2.13) confirms, as argued physically above, that $\eta(\tau)$ is initially negative, attains a minimum, and thereafter increases steadily. The minimum value of η is $-(\pi S)^{-1}$ and occurs at $\tau = 4\pi^{-1}$. In dimensional terms, the minimum, say $a_{\min}$, and the time, say $t_{\min}$, at which this occurs are given by

$$a_{\min} = \frac{-k^2(T_f - T_0)^2}{\pi\rho\kappa HL}, \quad t_{\min} = \frac{k^2(T_f - T_0)^2}{\pi\kappa H^2}. \tag{2.14a, b}$$

The solutions (2.12) and (2.13) could not be expected to be valid for $\tau \gg 1$, or alternatively for $t \gg t_{\min}$, but should provide reasonable approximations for t of order $t_{\min}$ or less, if $a_{\min}$ is sufficiently small. Expressed differently, the solutions represent useful approximations for $\tau < \tau_c(S)$, for some τ_c which is an increasing function of S. In particular, we shall show below that (2.13) is a good approximation for all τ in the limit of large S. On a point of analysis, it might be of interest to note that the solutions for large S in *finite* domains are easily obtained by neglecting T_t to lowest order in (2.2) (see, for example Hill 1987, Chapter 2). It is not possible to apply this approach immediately in the semi-infinite domain considered here.

The complete solution to (2.8)–(2.11) can be obtained numerically in a straightforward way after introducing the moving coordinate axis (Landau 1950)

$$z = \xi - \eta(\tau), \tag{2.15}$$

which moves the (unknown) position of the boundary to $z = 0$. In terms of z the equations become

$$\theta_\tau = \dot{\eta}(\tau)\,\theta_z + \tfrac{1}{4}\theta_{zz} \quad (z > 0), \tag{2.16}$$

$$\theta = 1, \quad 4S\dot{\eta} = 1 + \theta_z \quad (z = 0), \tag{2.17a, b}$$

$$\theta \to 0 \quad (z \to \infty), \tag{2.18}$$

$$\theta = 0 \quad (\tau = 0, \quad z > 0), \tag{2.19}$$

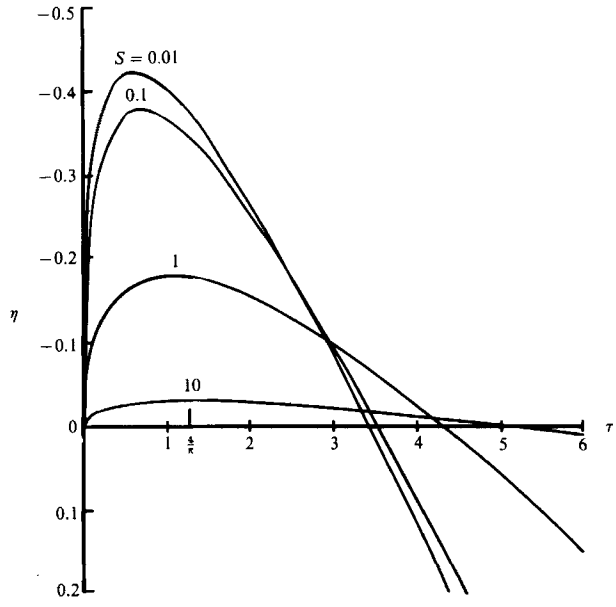

FIGURE 3. The non-dimensional position of the moving interface, η, as a function of the non-dimensional time, τ, for $S = 0.01$, 0.1, 1 and 10 and $T_m = T_l$. The point $\tau = 4/\pi$, where η attains a minimum in the limit of large S, is marked.

which can be solved by an explicit finite-difference scheme, as described by Landau (1950). In order to initiate the numerical solution, a series representation in powers of $\tau^{\frac{1}{2}}$ was developed. In the limit $S \to \infty$ the first terms in the expansion are of course given by (2.12) and (2.13). Note that $\dot{\eta}$ initially has a square-root singularity which balances the initially infinite value of θ_ξ in (2.9*b*). The determination of the complete expansion, its convergence and some other properties are discussed in Appendix A, followed by a discussion of the numerical scheme and its convergence in Appendix B.

Figure 3 presents graphs of $\eta(\tau)$ for four values of S. Only for $S = 10$ is (2.13) at all a good approximation. The values of the minimum of η, say $\eta_{\min}$, and the value of τ at which this is attained, say $\tau_{\min}$, are plotted in figure 4, which also includes the results obtained by the linearized procedure described above. Figure 5 presents the (non-zero) value of τ at which $\eta = 0$, say τ_0, and also $\tau_{\min}$ for comparison.

A τ-independent solution of (2.16)–(2.19) can be obtained by suppressing θ_τ in (2.16) and setting $\dot{\eta}$ to a constant, say V. Then the solution of (2.16), (2.17*a*) and (2.18) is

$$\theta(z) = \exp(-4Vz), \tag{2.20}$$

which satisfies (2.17*b*) if

$$V = \frac{1}{4(1+S)}. \tag{2.21}$$

The steady-state solution (2.20) and (2.21) of course do not satisfy the initial condition (2.19). It is argued in Appendix C that (2.20) and (2.21) represent the solution for large τ no matter what the initial condition. This steady-state solution is the one used in the previous papers on Archaen lava flows which were referred to in the Introduction.

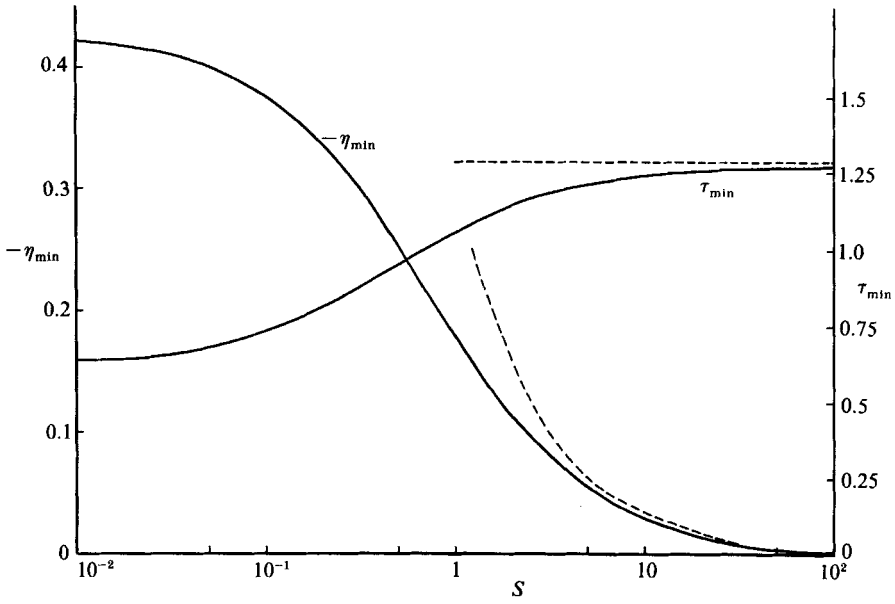

FIGURE 4. The largest value of the non-dimensional chill thickness, $-\eta_{min}$, and the non-dimensional time at which this is attained, τ_{min}, as functions of the Stefan number S for $T_m = T_t$. The dashed curves correspond to $\eta_{min} = -(\pi S)^{-1}$ and $\tau_{min} = 4\pi^{-1}$, which are the results obtained by applying the boundary conditions of fixed temperature and conservation of heat at $\xi = 0$ rather than at the moving interface $\xi = \eta$.

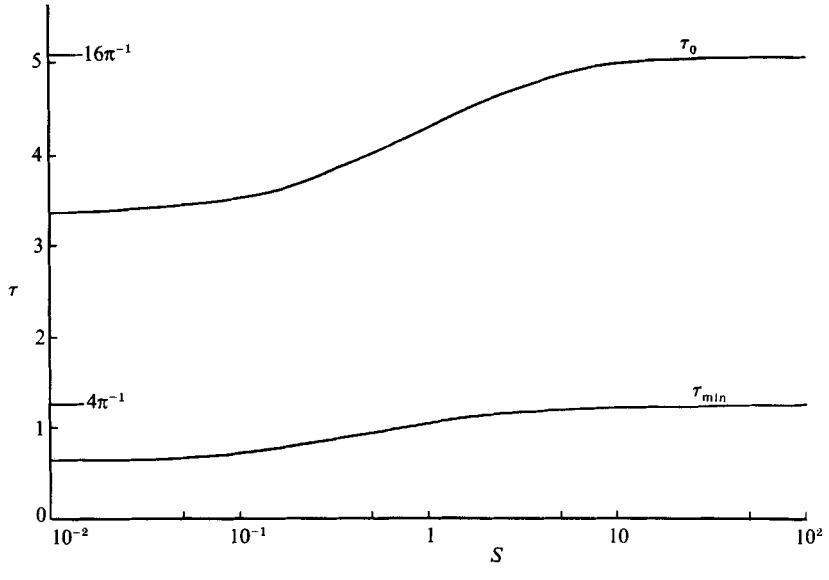

FIGURE 5. The non-dimensional time taken for the chilled margin to melt totally, τ_0, as a function of the Stefan number S for $T_m = T_t$. The value of τ_{min} from figure 3 is redrawn for comparison purposes. The limits as $S \to \infty$ of $16\pi^{-1}$ and $4\pi^{-1}$ for τ_0 and τ_{min}, respectively, are indicated on the ordinate.

3. Freezing temperature less than initial temperature of solid

In this case, for which $T_f \leqslant T_0 (< T_m)$, and which is sketched in figure 6(*a*, *b*), the fluid can never freeze. The temperature at the interface, T_i, at $t = 0+$ must be T_0. Any greater temperature would imply a very large conductive heat flux into the solid that could not be balanced since there is now no latent-heat release. As the conductive profile develops, T_i rises until either $T_i = T_m$, beyond which time the solid melts (figure 6*b*); or if $T_\infty \leqslant T_m$, $T_i \to T_\infty$ as $t \to \infty$ and there is no melting at all (figure 6*a*).

In order to carry out a quantitative analysis, we assume that

$$H = h(T_\infty - T_i), \tag{3.1}$$

where h (the heat-transfer coefficient) is a constant, in line with the standard formulation for turbulent flows over solid boundaries (Savino & Siegel 1969 and Holman 1976). The governing equations can then be obtained from (2.2)–(2.5) by setting $a \equiv 0$ and $T_f = T_i$ with H given by (3.1).

Introducing the non-dimensional variables

$$T = T_0 + (T_m - T_0)\psi, \quad T_i = T_0 + (T_m - T_0)\psi_i, \tag{3.2a, b}$$

$$x = \frac{k}{\alpha h}\zeta, \quad t = \frac{1}{4}\frac{k^2}{\alpha^2 \kappa h^2}\sigma, \tag{3.2c, d}$$

where

$$\alpha = (T_\infty - T_m)/(T_m - T_0), \tag{3.3}$$

with $-1 < \alpha < \infty$, we can express the problem as

$$\psi_\sigma = \tfrac{1}{4}\psi_{\zeta\zeta} \quad (\zeta > 0), \tag{3.4}$$

$$\psi = \psi_i, \quad \alpha\psi_\zeta = \psi_i - 1 - \alpha \quad (\zeta = 0, \quad \sigma < \sigma_{melt}), \tag{3.5a, b}$$

$$\psi \to 0 \quad (\zeta \to \infty), \tag{3.6}$$

$$\psi = 0 \quad (\sigma = 0, \quad \zeta > 0), \tag{3.7}$$

where σ_{melt} is the value of σ for which $\psi_i = 1$; alternatively it is the non-dimensional time at which $T_i = T_m$ and melting commences. If $T_\infty < T_m$, or $\alpha < 0$, that time never occurs. Equation (3.5*b*) expresses the heat flux from the fluid as a function of the (unknown) temperature at the interface. The standard solution for a semi-infinite solid subject to a prescribed heat flux at the boundary (Carslaw & Jaeger 1959, p. 76) then leads to the integral equation

$$\psi_i(\sigma) = \frac{1}{2\alpha\pi^{\frac{1}{2}}}\int_0^\sigma [1 + \alpha - \psi_i(\lambda)](\sigma - \lambda)^{-\frac{1}{2}}\,d\lambda \tag{3.8a}$$

$$= \frac{1+\alpha}{\alpha\pi^{\frac{1}{2}}}\sigma^{\frac{1}{2}} - \frac{1}{2\alpha\pi^{\frac{1}{2}}}\int_0^\sigma \psi_i(\lambda)(\sigma - \lambda)^{-\frac{1}{2}}\,d\lambda. \tag{3.8b}$$

Taking the Laplace transform of both sides of (3.8*b*), using the convolution theorem and denoting the Laplace transform of $\psi_i(\sigma)$ by $\Psi(p)$, we obtain

$$\Psi(p) = \frac{1+\alpha}{p(1 + 2\alpha p^{\frac{1}{2}})}, \tag{3.9}$$

the inverse of which is

$$\psi_i(\sigma) = (1+\alpha)[1 - \exp(\tfrac{1}{4}\alpha^{-2}\sigma)\operatorname{erfc}(\tfrac{1}{2}\alpha^{-1}\sigma^{\frac{1}{2}})]. \tag{3.10}$$

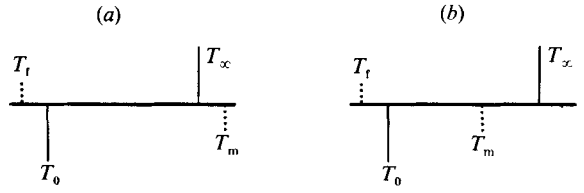

FIGURE 6. A sketch of the distribution of temperatures with $T_f < T_0$. In case (*a*) $T_\infty < T_m$ and the initially solid half-space can never melt, while in case (*b*) $T_m < T_\infty$ and it will melt.

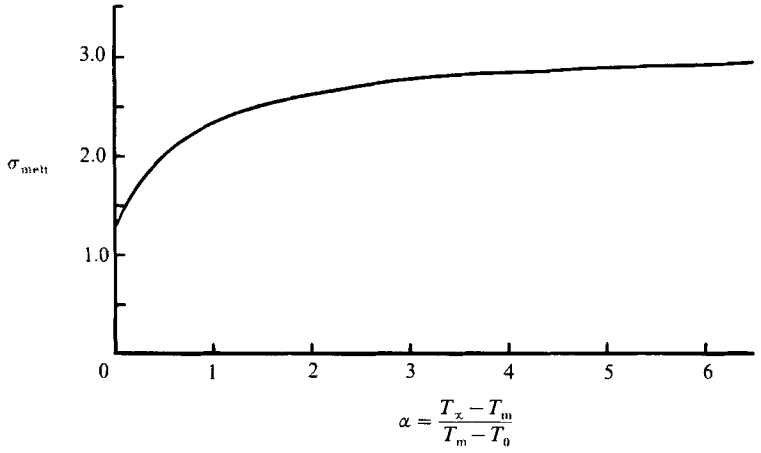

FIGURE 7. The non-dimensional time at which melting of the solid commences, for $T_f \leqslant T_0 < T_m$.

The value of σ_{melt} can then be determined from the numerical solution of

$$\exp(\tfrac{1}{4}\alpha^{-2}\sigma)\operatorname{erfc}(\tfrac{1}{2}\alpha^{-1}\sigma^{\frac{1}{2}}) = (1+\alpha^{-1})^{-1}, \tag{3.11}$$

the result of which is presented in figure 7. Note that although σ_{melt} is finite as $\alpha \to 0$, the corresponding dimensional time t_{melt} is infinite, because from (3.2*d*) $t_{melt} \propto \alpha^{-2}\sigma_{melt}$. Physically, for $\alpha = 0$, as t increases, $T_i \to T_m$ in such a way that $H \to 0$ sufficiently rapidly that the time taken for T_i to equal T_m is infinite. For $\alpha < 0$, σ_{melt} has no meaning, as has already been explained.

From the relationship (3.10) for ψ_i the solution for $\psi(\zeta, \sigma)$ can be obtained by inserting (3.10) into formula (9) of §2.9, Chapter II, of Carslaw & Jaeger (1959) and carrying out the integration to yield

$$\psi(\zeta,\sigma) = (1+\alpha)[\operatorname{erfc}(\zeta\sigma^{-\frac{1}{2}}) - \exp[\alpha^{-1}\zeta + \tfrac{1}{4}\alpha^{-2}\sigma]\operatorname{erfc}(\zeta\sigma^{-\frac{1}{2}} + \tfrac{1}{2}\alpha^{-1}\sigma^{\frac{1}{2}})]. \tag{3.12}$$

For $\sigma > \sigma_{melt}$, $T_i = T_m$ and melting of the solid occurs. Equations (3.5) and (3.7) are then replaced by

$$\psi_i = 1, \quad 4S\dot{\eta} = 1 + \psi_\zeta \quad (\zeta = \eta(\sigma)), \tag{3.13a, b}$$

$$\psi = \psi(\zeta, \sigma_{melt}) \quad (\sigma = \sigma_{melt}, \quad \zeta > 0), \tag{3.14}$$

where $\eta(\sigma)$ and S are as in (2.6*d*) and (2.7) with T_m replacing T_f and $\psi(\zeta, \sigma_{melt})$ is determined from (3.12). The system (3.4), (3.6), (3.13) and (3.14) can then be integrated numerically by using the Landau transformation (2.15) and the numerical scheme discussed in Appendix B. Some typical results are shown in figure 8. The plots indicate that the non-dimensional melt rate approaches a constant value,

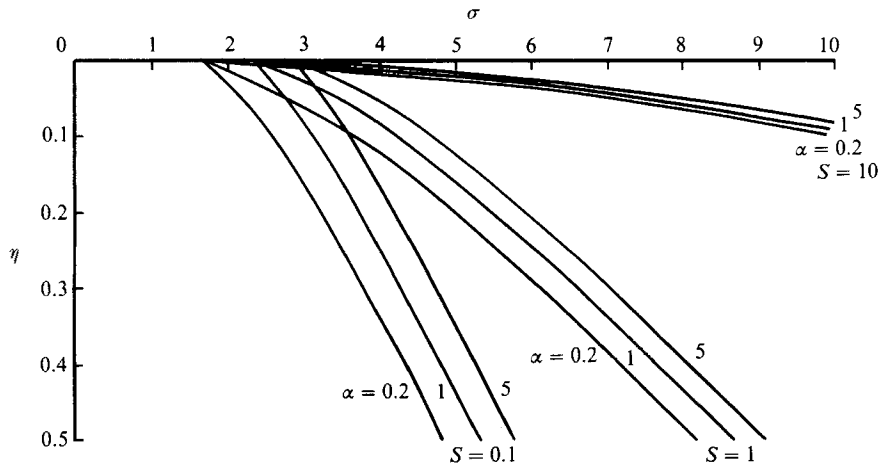

FIGURE 8. The non-dimensional position of the interface between the turbulent flow and the solid, η, as a function of the non-dimensional time, σ, for Stefan numbers $S = 0.1$, 1 and 10 and $\alpha = (T_\infty - T_m)/(T_m - T_0) = 0.2$, 1 and 5, for $T_f \leqslant T_0 < T_m < T_\infty$.

independent of α, fairly quickly in a timescale that is an increasing function of S. This is because α appears only in the initial condition (3.14) and the derivative term, $\dot{\eta}$, in (3.13*b*) is premultiplied by S.

4. Freezing temperature greater than initial temperature of solid but less than melting temperature

In this case, for which $T_0 < T_f < T_m$, and which is sketched in figure 9, the fluid again first freezes and forms a chill. After a time, the chill reaches a maximum thickness and then melts until the initial solid surface is recovered. The interfacial temperature, T_i, subsequently increases. If $T_m < T_\infty$ (figure 9*b*) T_i attains the value of T_m in finite time and thereafter the solid melts continually. If $T_\infty \leqslant T_m$ (figure 9*a*) $T_i \to T_\infty$ as $t \to \infty$ and no melting occurs.

The governing equations are (2.2), (2.4), (2.5) in addition to

$$\text{for} \quad 0 \leqslant t < t_0: \quad T = T_f \quad \text{and} \quad \rho L\dot{a} = H_f + kT_x \quad (x = a(t)), \qquad (4.1a, b)$$

$$\text{for} \quad t_0 \leqslant t < t_1: \quad T = T_i \quad \text{and} \quad 0 = H_f\left(\frac{T_\infty - T_i}{T_\infty - T_f}\right) + kT_x \quad (x = 0), \qquad (4.2a, b)$$

$$\text{for} \quad t_1 \leqslant t: \quad T = T_m \quad \text{and} \quad \rho L\dot{a} = H_f\left(\frac{T_\infty - T_m}{T_\infty - T_f}\right) + kT_x \quad (x = a(t)), \qquad (4.3a, b)$$

where t_0 is the time taken for the chill to melt back completely ($a(t_0) = 0$), t_1 is the time at which melting of the initial solid first occurs ($T_i(t_1) = T_m$), and $H_f = h(T_\infty - T_f)$. It will be convenient to introduce

$$\beta = (T_\infty - T_m)/(T_\infty - T_f), \qquad (4.4)$$

which is by hypothesis constrained by $-\infty < \beta < 1$. If $\beta \leqslant 0$ (figure 9*a*) T_i never attains the value T_m, melting does not occur and (4.3) is irrelevant.

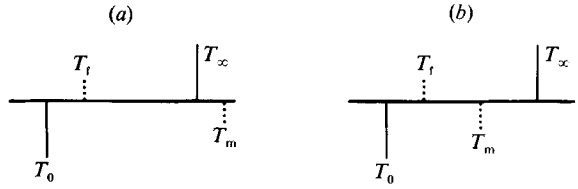

FIGURE 9. A sketch of the distribution of temperatures with $T_0 < T_f < T_m$. In case (*a*) $T_\infty < T_m$ and the initially solid half-space can never melt, while in case (*b*) $T_m < T_\infty$ and it will melt.

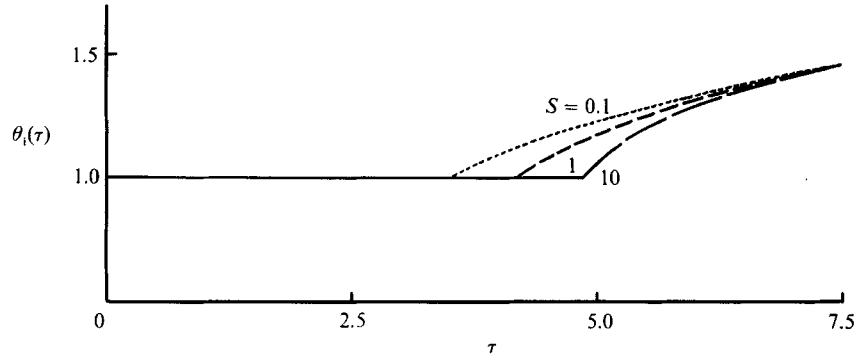

FIGURE 10. The non-dimensional temperature at the moving interface between the turbulent flow and the solidified chill, $\theta_i(\tau)$, as a function of the non-dimensional time, τ, for $\gamma = (T_f - T_0)/(T_\infty - T_f) = 0.2$ and $S = 0.1$, 1 and 10, for $T_\infty < T_m$. In the limit $\tau \to \infty, \theta_i(\tau) \to 1 + \gamma^{-1} = 6$.

Introducing non-dimensional variables as in (2.6) but replacing H by H_f, we obtain (2.8), (2.10) and (2.11) in addition to

$$\text{for} \quad 0 \leqslant \tau \leqslant \tau_0: \quad \theta = 1, \quad 4S\dot{\eta} = 1 + \theta_\xi \quad (\xi = \eta(\tau)), \tag{4.5a, b}$$

$$\text{for} \quad \tau_0 \leqslant \tau < \tau_1: \quad \theta = \theta_i, \quad \theta_\xi - \gamma\theta_i + 1 + \gamma = 0 \quad (\xi = 0), \tag{4.6a, b}$$

$$\text{for} \quad \tau_1 \leqslant \tau: \quad \theta = 1 + (1-\beta)\gamma^{-1}, \quad 4S\dot{\eta} = \beta + \theta_\xi \quad (\xi = \eta(\tau)), \tag{4.7a, b}$$

where

$$\gamma = (T_f - T_0)/(T_\infty - T_f), \tag{4.8}$$

which is by hypothesis positive. In this section it is convenient to consider β and γ as the two external parameters, but it could be borne in mind that γ is related to α and β by

$$\gamma = \alpha^{-1}\beta(1+\alpha) - 1. \tag{4.9}$$

Equation (4.6) is valid until T_i equals T_m, that is, until $\theta_i = 1 + (1-\beta)\gamma^{-1}$. But (4.6) indicates that the maximum possible value of θ_i is $1 + \gamma^{-1}$, which is attained as $\theta_\xi \to 0$. This confirms that if $\beta \leqslant 0$ no further melting occurs.

No parameters appear in (2.8), (2.10) and (2.11) and so from (4.5)–(4.7) we see that the system is described by the three parameters, S, β and γ.

If $\beta \leqslant 0$ only (4.5) and (4.6) are relevant and so the system is described by the two parameters S and γ only. Since (4.5) is identical in form to (2.9), the solution for $0 \leqslant \tau < \tau_0$ is identical to that already described in §2 and is independent of γ. For $\tau_0 < \tau$ both S and γ play a role. But since no melting takes place in this range, S does not appear in (4.6) and its value influences only the solution for τ close to τ_0. This is shown in figure 10 which plots the interfacial temperature $\theta_i(\tau)$ for three values of S at a fixed value of γ. It is seen that as τ increases, the curves come together.

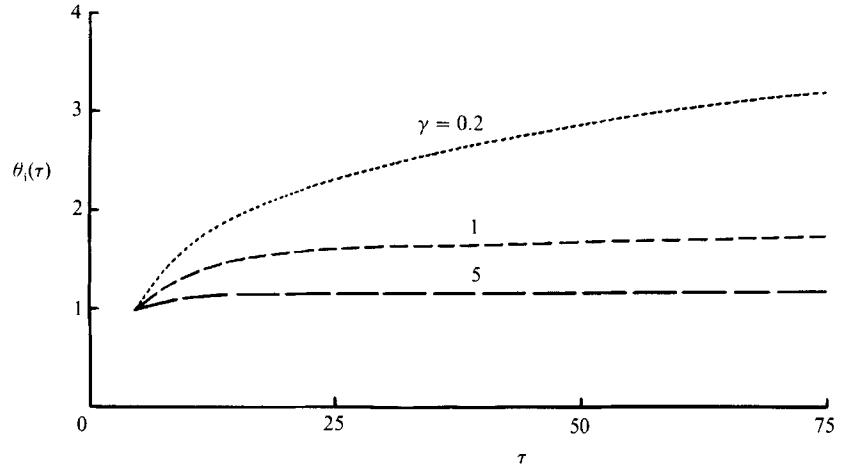

FIGURE 11. The non-dimensional temperature at the moving interface between the turbulent flow and the solidified chill, $\theta_i(\tau)$, as a function of the non-dimensional time, τ, for $S = 10$ and $\gamma = (T_f - T_0)/(T_\infty - T_f) = 0.2$, 1 and 5, for $T_\infty < T_m$. In the limit $\tau \to \infty, \theta_i(\tau) \to 1 + \gamma^{-1}$.

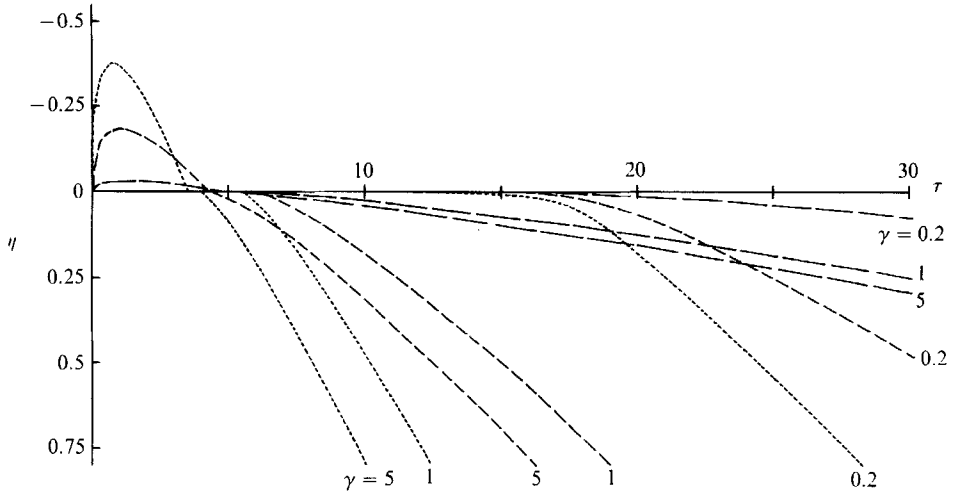

FIGURE 12. The non-dimensional position of the interface between the turbulent flow and the solid, η, as a function of the non-dimensional time, τ, for $S = 0.1$ (.....), 1(----) and 10 (——) and $\gamma = (T_f - T_0)/(T_\infty - T_f) = 0.2$, 1 and 5, for $T_0 < T_f < T_m < T_\infty$.

Figure 11 plots $\theta_i(\tau)$ for larger values of τ for three values of γ with $S = 10$, but, except near $\tau = \tau_0$, the curves would take the same form for all S.

If $0 < \beta < 1$ the solution is determined by all three parameters. The solution for $0 \leqslant \tau < \tau_0$, which is dependent only on S, has already been described. For $\tau_0 \leqslant \tau < \tau_1$ the solution is dependent mainly on γ and to some extent on S, as already discussed, with the value of β being relevant only in the determination of τ_1. Curves for the interfacial temperature in this range are hence identical to those plotted in figure 11 except that for $\tau_1 \leqslant \tau$, θ_i remains constant at $1 + (1-\beta)\gamma^{-1}$. Figure 12 plots $\eta(\tau)$ for three different values of both S and γ for $\beta = 0.8$. The portions for $\tau \leqslant \tau_0$ are independent of γ, as already described, and identical to the plots for figure 3. For $\tau_0 \leqslant \tau < \tau_1, \eta \equiv 0$. It can be seen from the figure that τ_1 increases as either S increases

or as γ decreases; and also, from the above discussion, as β decreases. For $\tau_1 < \tau$ each of S, β and γ play a role in the solution as can be seen from the figure and (4.7). The large-time asymptotic solution can be obtained, in a manner identical to that leading to (2.20) and (2.21), as

$$\theta(z) = [1+(1-\beta)\gamma^{-1}]\exp(-4Vz), \tag{4.10}$$

with

$$V = \frac{\beta}{4[1+S+(1-\beta)\gamma^{-1}]}. \tag{4.11}$$

For $\beta = 1$, $T_f = T_m$ and $\tau_1 = \tau_0$. Equation (4.6) is then inoperative and (4.5) and (4.7) are identical to each other and to (2.7). The system reverts exactly to that considered in §2.

5. Melting temperature less than freezing temperature

This case, for which $(T_0 <) T_m < T_f (< T_\infty)$ and which is sketched in figure 13, can be divided into two sub-cases depending on the value of S and

$$\delta = (T_m - T_0)/(T_f - T_0) = [1+\alpha\beta^{-1}(\beta-1)]^{-1}. \tag{5.1a, b}$$

The first sub-case occurs only for $\delta > 0.5$ and sufficiently small S, as sketched in figure 14. In this sub-case, the fluid initially forms a chill, as before. The temperature at the chill/solid interface is initially less than the melting temperature of the solid but gradually rises to it. Only then can melting of the original solid occur and the melting is postulated to take place underneath the solid chill. With time, the chill melts, as before. At this point we assume that the trapped fluid is instantaneously 'blown-off', or ablated, and melting of the solid half-space, now in contact with the turbulent flow, continues. An important assumption of this model is that the chill that is formed is sufficiently rigid to lie on a fluid layer while withstanding the buffeting from the turbulent flow above it. Depending on the material properties of the chill, this may not be possible. Another extreme is that the chill spontaneously breaks down on formation and is swept into the turbulent flow. There are also other possibilities, all of which might make interesting situations to analyse at some future date.

In the second sub-case, the original solid melts as soon as the turbulent flow is initiated and the chill forms. There are, for a time, two interfaces at which a phase change is occurring: one penetrates the turbulent flow while the other, beneath it, penetrates the original solid. The subsequent evolution of the system is qualitatively identical to that already described for the first sub-case.

The division between the two sub-cases occurs when the temperature at $\xi = 0$ and $\tau = 0+$ equals T_m. With the notation of Appendix A, the former is given by $T_0 + A_0(T_f - T_0)$. Thus the dividing curve is given by $\delta = (T_m - T_0)/(T_f - T_0) = A_0$, plotted in figure 14, and the first sub-case occurs in the region to the left of the curve.

Mathematically, the system is described in terms of the non-dimensionalization (2.6) and the representations $\eta_U(\tau)$ and $\eta_L(\tau)$ for the upper and lower interfaces, respectively, as

$$\theta_\tau = \tfrac{1}{4}\theta_{\xi\xi} \quad (\xi > \eta_U(\tau) \quad \text{for} \quad 0 < \tau < \tau_0, \quad \text{and} \quad \xi > \eta_L(\tau) \quad \text{for} \quad \tau_0 < \tau), \tag{5.2}$$

$$\text{for} \quad 0 < \tau < \tau_0: \quad \theta = 1 \quad \text{and} \quad 4S\dot{\eta}_U = 1 + \theta_\xi \quad (\xi = \eta_U(\tau)), \tag{5.3a, b}$$

$$\text{for} \quad \tau_1 < \tau < \tau_0: \quad \theta = \delta \quad \text{and} \quad 4S\dot{\eta}_L = \theta_\xi|_+ - \theta_\xi|_- \quad (\xi = \eta_L(\tau)), \tag{5.4a, b}$$

$$\text{for} \quad \tau_0 < \tau: \quad \theta = \delta \quad \text{and} \quad 4S\dot{\eta}_L = \beta + \theta_\xi \quad (\xi = \eta_L(\tau)), \tag{5.5a, b}$$

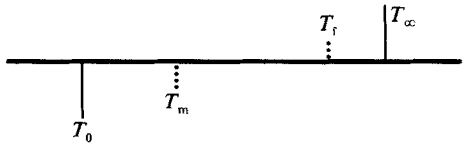

FIGURE 13. A sketch of the distribution of temperatures with $T_m < T_f$.

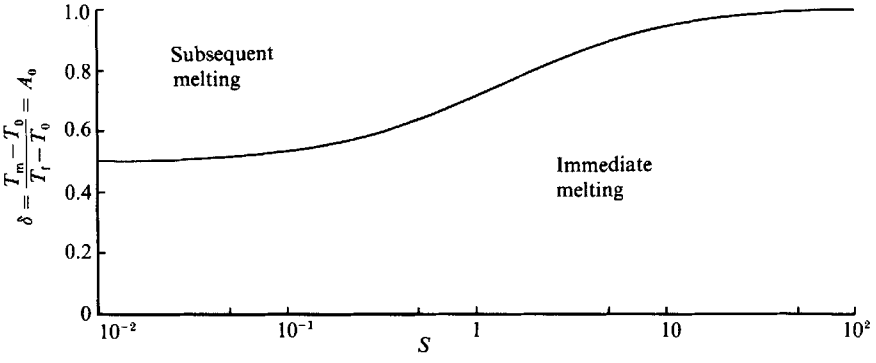

FIGURE 14. The curve of $\delta = (T_m - T_0)/(T_f - T_0)$ as a function of the Stefan number S which separates the regions in which the initial solid melts immediately (on the right) from that in which some time elapses after the initiation of the turbulent flow before melting commences (on the left) for $T_0 < T_m < T_f < T_\infty$.

in addition to the initial and far-field conditions (2.10) and (2.11), where in the second sub-case $\tau_1 \equiv 0$.

Because there are now two unknown, moving boundaries, the numerical solution of (2.10), (2.11) and (5.2)–(5.4) has to be approached in a slightly different manner than for the previous calculations. We introduce a new coordinate

$$y = [\xi - \eta_U(\tau)]/[\eta_L(\tau) - \eta_U(\tau)], \tag{5.6}$$

so that for $\tau_1 < \tau < \tau_0$ the region between the moving interfaces is mapped onto $(0, 1)$. In terms of y the system becomes

$$\theta_\tau = \{\dot\eta_U(\tau) + y[\dot\eta_L(\tau) - \dot\eta_U(\tau)]\}[\eta_L(\tau) - \eta_U(\tau)]^{-1}\theta_y + \tfrac{1}{4}[\eta_L(\tau) - \eta_U(\tau)]^{-2}\theta_{yy}, \tag{5.7}$$

$$\theta = 1, \quad 4S\dot\eta_U = 1 + [\eta_L(\tau) - \eta_U(\tau)]^{-1}\theta_y \quad (y = 0) \tag{5.8}$$

$$\text{for} \quad \tau_1 < \tau < \tau_0\text{:} \quad \theta = \delta, \quad 4S\dot\eta_L[\eta_L(\tau) - \eta_U(\tau)] = \theta_y|_+ - \theta_y|_- \quad (y = 1), \tag{5.9}$$

together with the appropriate initial and far-field conditions. This system can then be integrated numerically in a quite straightforward way using the same techniques as those discussed in Appendix B.

If $\tau_0 \equiv 0$ (the second sub-case), there is a singularity in both η_U and η_L at $\tau = 0$. Thus an analytical solution to the equations must be obtained which is valid for small τ and can be used as an initial input to the numerical scheme. The procedure that obtains a power-series representation in $\tau^{\frac{1}{2}}$ is explained in Appendix D. Similar expansions have been obtained by Tao (1978).

It might be anticipated that the first two terms in the power-series representations of $\eta_U(\tau)$ and $\eta_L(\tau)$ for large S would yield a useful approximation, just as in §2. These cannot be obtained directly, by the procedure of determining the solution of an appropriately linearized system, as in §2, because then both the different boundary

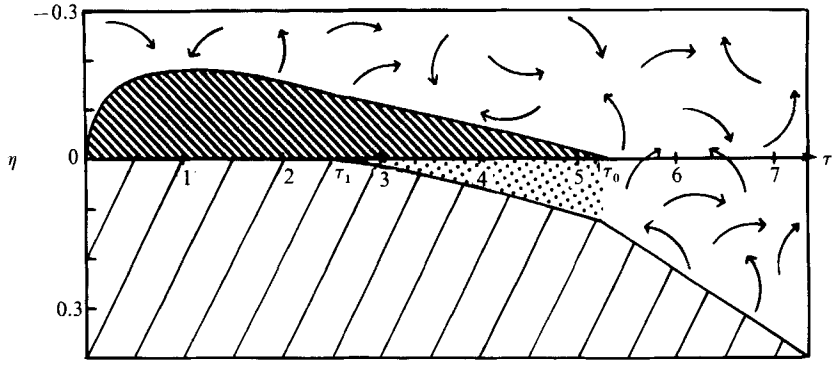

FIGURE 15. The non-dimensional interfaces between the turbulent flow, chill, melt and original solid for $S = 1$, $\beta = \frac{4}{3}$ and $\delta = 0.75$, for $T_0 < T_m < T_f < T_\infty$ with the same designation as in figure 1 with the addition of ▨ as the unmelted original solid.

conditions (5.3) and (5.4) would have to be satisfied at the same point $\xi = 0$. Nevertheless they can be obtained from the expansion, as outlined in Appendix D. The results are

$$\eta_U(\tau) \approx -\tfrac{1}{2}(1-\delta)^{\frac{1}{2}}(\tau/S)^{\frac{1}{2}} + \tfrac{5}{24}(\tau/S) \tag{5.10}$$

and

$$\eta_L(\tau) \approx \tfrac{1}{2}(1-\delta)^{\frac{1}{2}}(\tau/S)^{\frac{1}{2}} + \tfrac{1}{24}(\tau/S). \tag{5.11}$$

Two important points emerge on comparing (5.10) and (2.13). First, the leading term in (5.10) is of order $S^{-\frac{1}{2}}$ (in contrast with order S^{-1} for the corresponding term in (2.13)). This reflects the fact that the melting, lower interface absorbs latent heat which must be balanced by an increased rate of freezing at the upper interface. Secondly, the expansion appears actually to be in powers of (τ/S) and hence will not yield useful results concerning the minima of $\eta_U(\tau)$ or the value of τ_0. All useful results follow from numerical integration. We shall commence by discussing the first sub-case, then the second before presenting a graph which connects the two. We end this section with a description of a simple laboratory experiment demonstrating that simultaneous freezing and melting can occur.

5.1. *The first sub-case* ($A_0 < T_m$)

A typical solution for $S = 1$, $\beta = \frac{4}{3}$ and $\delta = 0.75$ is plotted in figure 15, along with special shading to highlight the different phases. For $\tau < \tau_1$ the solution is exactly as described in §2. At $\tau = \tau_1$ melting of the initial solid commences at $\xi = 0$. The extraction of latent heat at the lower boundary slows down the tendency for the chill to melt. Consequently there is a discontinuous decrease of $\dot{\eta}_U(\tau)$ at $\tau = \tau_1$ and the value of τ_0 is increased over that presented in figure 5. With increasing S, τ_0 increases monotonically owing to the increasing amount of latent heat absorbed at the lower interface (see figure 16). There is in addition an increase of τ_0 as δ decreases, as is indicated on the figure also. The temperature profile in the melted phase decreases downwards and hence is stable. Indeed, the thermal timescale for conduction over the distance $(\eta_L - \eta_U)$ is so much less than $(\tau_0 - \tau_1)$ that to a good degree of approximation the temperature profile in $\eta_U \leqslant \xi \leqslant \eta_L$ is a straight line joining the boundary temperatures 1 and δ.

At τ_1 the chill has completely melted and we assume that the melt layer that was trapped until this time is instantaneously 'blown-off', or ablated, and mixes with the overriding turbulent flow. The lower interface experiences a larger heat flux,

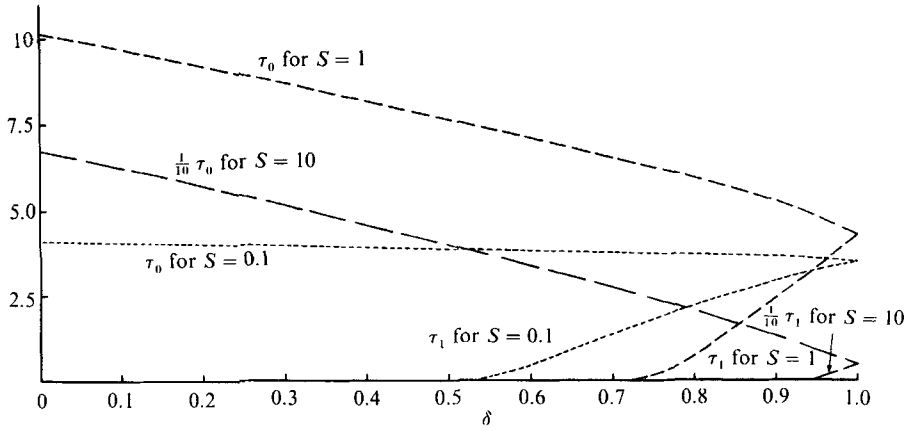

FIGURE 16. The non-dimensional times at which melting of the original solid commences, τ_1, and melting of the chill is completed, τ_0, as a function of δ for $S = 0.1$ (...), 1 (----), and 10 (——), for $T_0 < T_m < T_f < T_\infty$. Note that $0.1\tau_0$ and $0.1\tau_1$ are plotted for $S = 10$.

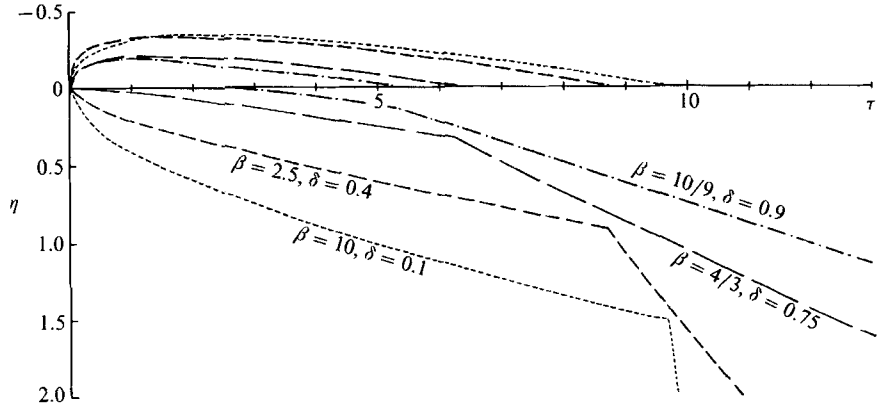

FIGURE 17. The non-dimensional interfaces between turbulent flow, chill, melt and original solid for $\beta = 10$ and $\delta = 0.1$; $\beta = 2.5$ and $\delta = 0.4$; $\beta = \frac{4}{3}$ and $\delta = 0.75$; and $\beta = \frac{10}{9}$ and $\delta = 0.9$ and $S = 1$, for $T_0 < T_m < T_f < T_\infty$.

according to the lower melting temperature, and begins to melt more rapidly at a rate that is an increasing function of β. The final rate of melting can be obtained by comparing (4.7), (4.10) and (5.5) to yield

$$V = \frac{\beta}{4(\delta + S)}. \tag{5.12}$$

5.2. *The second sub-case* ($A_0 > T_m$)

In this case melting of the initial solid occurs immediately, while a chill is formed above the resultant stable melt layer. The melting at the lower interface increases the time taken for the chill to melt and this increase is quite considerable for large values of S, as shown in figure 16. Two typical solutions, both for $S = 1$, with $\beta = 10$, $\delta = 0.1$ and $\beta = 2.5$, $\delta = 0.4$, are plotted in figure 17 along with two solutions of the first sub-case, again with $S = 1$, but with $\beta = \frac{4}{3}$, $\delta = 0.75$ and $\beta = \frac{10}{9}$, $\delta = 0.9$.

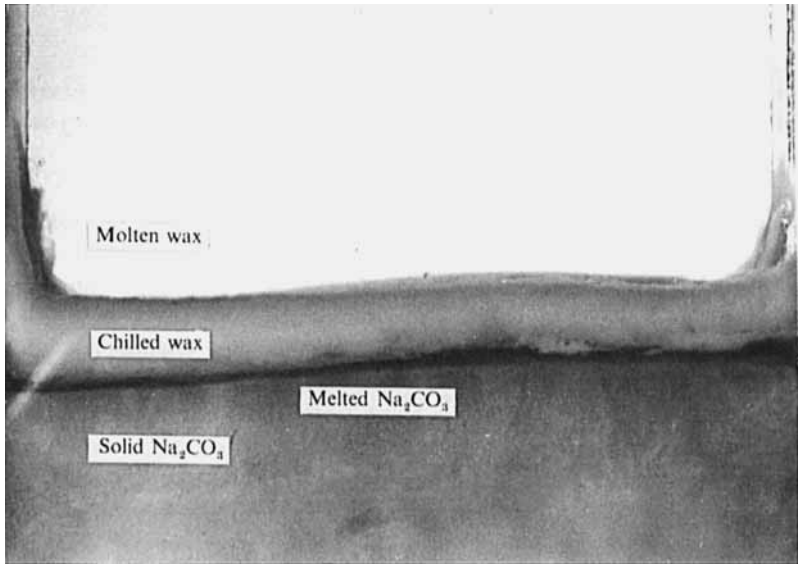

FIGURE 18. A photograph of the laboratory experiment in which hot, molten wax was poured over solid Na_2CO_3 of eutectic composition. The wax chilled at the same time as the solid Na_2CO_3 melted.

5.3. *Experimental investigation*

It is of interest to examine experimentally the concept that a hot flow can solidify while the cold solid beneath it melts. Accordingly, with my graduate research assistant, M. A. Hallworth, I conducted the following simple experiment. A Perspex container $5 \times 15 \times 25$ cm high was half-filled with a lightly blue-dyed, eutectic composition of aqueous sodium carbonate (Na_2CO_3), which has a freezing temperature of -2.1 °C and a liquid density at that temperature of 1.06 g cm^{-3}. The solution was frozen overnight in a commercial freezer and reached a temperature of approximately -15 °C. We filled the remainder of the container with molten Polyethylene glycol 600 (PEG), which has a commercially quoted melting range of 20–25 °C and a density of 1.12 g cm^{-3} just above that temperature. The PEG was only a few degrees above 25 °C.

As can be seen in figure 18, the PEG did indeed form a chill, while at the same time a eutectic Na_2CO_3 melt layer formed beneath it. (The visual evidence was abundantly clear and much better than the photograph.) The set-up of the experiment was not identical to the theoretical model considered here in that there was no turbulent flow in the fluid layer. Nevertheless it suffices to confirm the essential concept that solidification and melting can occur simultaneously.

6. Conclusions

The main conclusion of the present calculations is that whenever a hot, turbulent flow is confined by a solid surface, the initial response is the formation of a chill if the freezing temperature of the fluid exceeds the initial temperature of the solid. If, further, the turbulent flow is sufficiently deep, as is the case assumed herein, the chill will melt back with time. Melting of the solid will then follow, as long as the melting

temperature is less than that of the turbulent flow. In all our analyses, the maximum thickness of the chill scales with

$$k^2(T_f - T_0)^2/\rho\kappa HL, \tag{6.1}$$

with a premultiplicative constant which is close to unity and is determined by the initial, freezing and melting temperatures of the fluid and solid. The corresponding timescale is

$$k^2(T_f - T_0)^2/\kappa H^2, \tag{6.2}$$

although the premultiplicative constant can be quite large. (Exact values are included in the figures.) Subsequent melting of the original solid can be quite accurately quantified by neglecting all this initial response and using the steady-state solution (2.20) and (2.21) and their equivalents.

Using typical values of the parameters as reported in Huppert *et al.* (1984) to describe the Archaen lava flows discussed in the Introduction, we find that the chilled margin grows to a thickness less than 1 cm. This is very much less than the thickness of the lava flows, which are believed to have been between 0.5 and 10 m. The calculated timescale for the formation and subsequent remelting of the chilled margin is of the order of 30 s. This is very much less than the typical flow time of the lavas, which is believed to have been days or possibly even weeks. This justifies the use of the long-time solutions (2.20) and (2.21) in the geological context.

While this work has been directed explicitly towards the passive convection of heat by forced turbulent streams, the ideas carry over to thermally or compositionally driven turbulent convective flows. The heat-transfer relationship in the general form (2.1) will still be valid, but the linear form (3.1), which we used in some of the calculations, will not. It may need to be replaced by the four-thirds relationship (Turner 1973)

$$H \propto (T_\infty - T_i)^{\frac{4}{3}}, \tag{6.3}$$

as was done in Huppert & Sparks (1988). Carrying out the above calculations for this nonlinear heat-transfer relationship would be relatively straightforward, but would involve more numerical computation.

It would be particularly interesting from a general fluid-mechanical point of view, and also geologically relevant, to extend the analysis to consider the turbulent flow to be of finite extent and to cool down as the chill is formed and possibly melts back. An interesting question to ask then is what are the conditions for which the turbulent flow does not contain sufficient thermal energy to permit the original solid to be melted. Under even more stringent conditions, the chill itself will not be melted, but will continue to grow and engulf the flow.

It would also be of interest to investigate the effects of a melting and freezing temperature *range*, rather than assuming, as was done herein, that melting and freezing take place at a fixed temperature. Of more mathematical concern, the calculations could be extended to investigate the effects of unequal fluid and solid properties, such as latent and specific heats.

I have benefitted from a number of stimulating conversations with Steve Sparks, who has awaited the appearance of this paper with feelings which have alternated between patience and exasperation since early 1985 when I first told him of the results presented in §2. I am grateful to Joyce Wheeler, who carefully carried out all the numerical calculations reported here and prepared some of the graphs for publication, and to Mark Hallworth, who helped me with the experiment and also prepared some graphs for publication. A discussion with Grae Worster about

numerical techniques was helpful, as was one with John Ockendon, who directed me to some of the references cited herein. Useful comments were made on an earlier draft by P. M. Bruce, D. T. Leighton, R. S. J. Sparks, A. W. Woods and M. G. Worster, to whom I am grateful. My research is supported generously by a grant from the BP Venture Research Unit.

Appendix A. The series solution

One method of solution of (2.8)–(2.11) is to use the embedding technique (Crank 1984) which expresses the solution of the differential equation and some of the boundary conditions in terms of (the unknown) $\theta(0,\tau)$ and then closes the system by determining the value of $\theta(0,\tau)$ to satisfy the remaining boundary condition(s). In Appendix C we express this solution in terms of an integral representation and use it to determine the solution for large τ. However, as explained there, the representation is invalid when η is negative, that is for $\tau \leqslant \tau_0$, and hence cannot be used to start the solution from $\tau = 0$. To do this we express $\theta(0,\tau)$ as a power series in $\tau^{\frac{1}{2}}$ in the form

$$\theta(0,\tau) = \sum_{n=0}^{\infty} \theta_n \tau^{\frac{1}{2}n}. \tag{A 1}$$

Equations (2.8), (2.10) and (2.11) are then satisfied by (Carslaw & Jaeger 1959, p. 63)

$$\theta(\xi,\tau) = \sum_{n=0}^{\infty} \theta_n \Gamma(\tfrac{1}{2}n+1)(4\tau)^{\frac{1}{2}n} i^n \operatorname{erfc}(\xi/\tau^{\frac{1}{2}}), \tag{A 2}$$

where $i^n \operatorname{erfc}(x)$ are the repeated integrals of the error function (Abramovitz & Stegun 1964). Inserting (A 2) into (2.9), we obtain the nonlinear differential equation

$$4S\dot{\eta} = 1 - \sum_{n=0}^{\infty} A_n \tau^{\frac{1}{2}(n-1)} i^{n-1} \operatorname{erfc}[\eta(\tau)/\tau^{\frac{1}{2}}] \tag{A 3}$$

subject to the constraint

$$\sum_{n=0}^{\infty} A_n \tau^{\frac{1}{2}n} i^n \operatorname{erfc}[\eta(\tau)/\tau^{\frac{1}{2}}] = 1, \tag{A 4}$$

where we have written A_n in place of $2^n\Gamma(\frac{1}{2}n+1)\theta_n$. Equations (A 3) and (A 4) can now be solved formally by inserting the expression

$$\eta(\tau) = \sum_{n=1}^{\infty} \eta_{n-1} \tau^{\frac{1}{2}n} \tag{A 5}$$

into them and equating like terms in $\tau^{\frac{1}{2}}$ one-by-one.

The lowest-order equations are

$$\pi^{\frac{1}{2}} S\eta_0 + A_0 \exp(-\eta_0^2) = 0 \tag{A 6}$$

and

$$A_0 \operatorname{erfc}(\eta_0) = 1, \tag{A 7}$$

which indicate that η_0 satisfies

$$\eta_0 \exp(\eta_0^2) \operatorname{erfc}(\eta_0) = -\frac{1}{\pi^{\frac{1}{2}} S}. \tag{A 8}$$

Relationships of the form (A 8) occur frequently in conductive problems involving phase changes and its solution is presented (graphically) in Carslaw & Jaeger (1959, figure 38). The equations giving A_n and η_n for $n = 0$–7 are presented in a document held in the *Journal of Fluid Mechanics* office and obtainable from there on request.

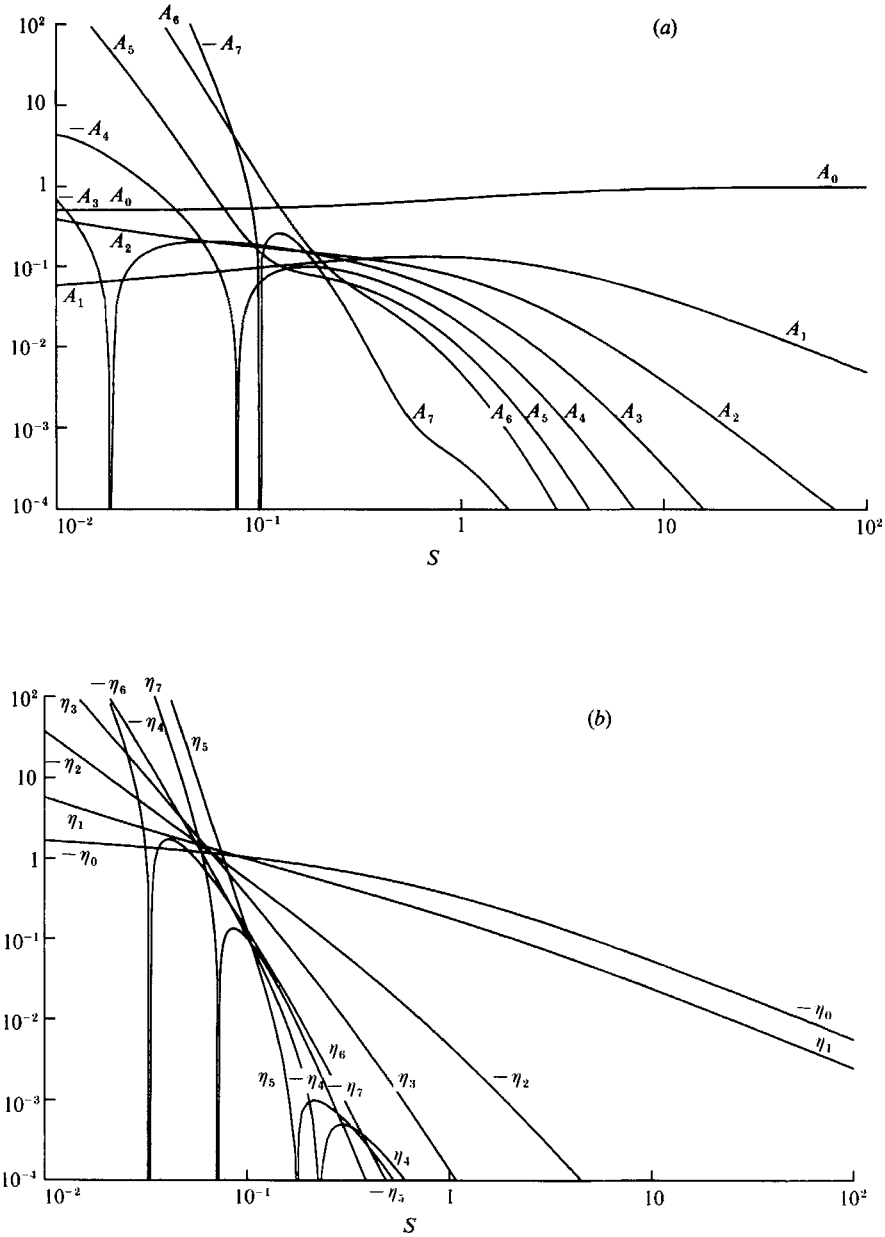

FIGURE 19. Curves of (*a*) A_n and (*b*) η_n for $n = 0$ to 7 as functions of S.

Figure 19 presents plots of A_n and η_n ($n = 0$–7) as functions of S. It is seen that for S greater than about 1, the A_n and η_n decay quite rapidly with increasing n, which suggests that for S greater than 1, the series representations (A 2) and (A 5) are quite rapidly convergent. For S much less than 1, on the other hand, both A_n and η_n become very badly behaved functions of n.

It might be thought that a useful representation for $\eta(\tau)$ could be obtained by using Padé approximates. Since η becomes linear in τ for large τ, as indicated in (2.21)

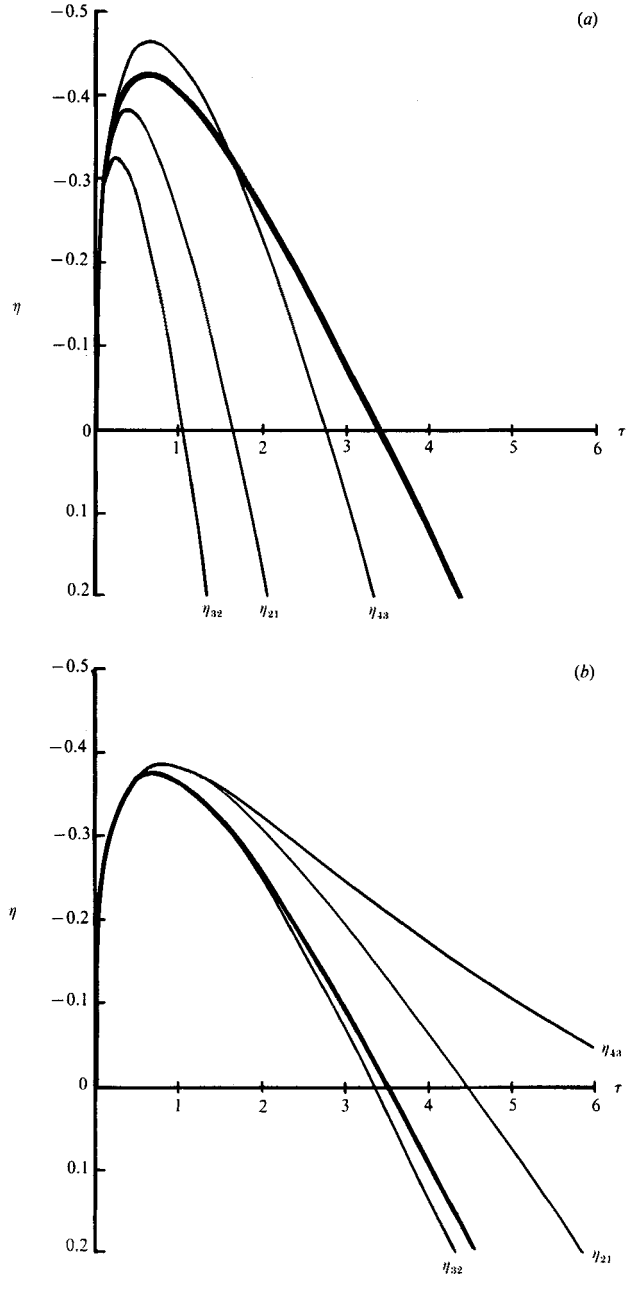

FIGURE 20. Curves of the Padé approximates η_{21}, η_{32} and η_{43} as a function of τ for (*a*) $S = 0.01$ and (*b*) 0.1. The thickened curves are the numerical solutions.

and demonstrated in Appendix C, an apparently sensible series of representations can be written as

$$\eta_{m+1,\,m}(\tau) = \frac{\eta_0 \tau^{\frac{1}{2}}\left(1 + \sum_{n=1}^{m+1} P_n \tau^{\frac{1}{2}n}\right)}{\left(1 + \sum_{n=1}^{m} Q_n \tau^{\frac{1}{2}n}\right)}, \tag{A 9}$$

where the B_n and C_n are determined by equating the $2m+1$ terms of lowest order in (A 5) and (A 9) in the usual way. The results of such a procedure are contained in the document obtainable from the *Journal of Fluid Mechanics* office. For largish values of S even a low-order Padé approximate gives good agreement with the numerical solution. In contrast, figure 20 presents plots of $\eta_{2,1}(\tau)$, $\eta_{3,2}(\tau)$ and $\eta_{4,3}(\tau)$ for $S = 0.01$ and 0.1 as well as the numerical solutions. The comparisons are not very encouraging.

We conclude that the series representation is suitable for use at small τ to initiate the numerical scheme but, especially for small S, it cannot be used to evaluate $\eta(\tau)$ even up to $\tau = \tau_{\min}$.

Appendix B. The numerical scheme, its convergence and stability

B.1. *The numerical scheme*

The system (2.16)–(2.19) was solved numerically using the following finite-difference scheme. With grid points along the z-axis at $z = ph$ $(p = 0, 1, \ldots, P)$ and along the τ-axis at $\tau = qk$ $(q = 0, 1, \ldots)$, we can determine the relationship for $\theta(p, q+1)$ in terms of $\theta(p-1, q)$, $\theta(p, q)$ and $\theta(p+1, q)$ from (2.16) as

$$\theta(p,q+1) = \theta(p,q) = \frac{1}{2}\left(\frac{k}{h}\right) V(q)\,[\theta(p+1,q) - \theta(p-1,q)]$$

$$+\frac{1}{4}\left(\frac{k}{h^2}\right)[\theta(p+1,q) - 2\theta(p,q) + \theta(p-1,q)], \quad (p = 1, 2, \ldots, P-1), \tag{B 1}$$

where

$$V(q) = \dot{\eta}(qk). \tag{B 2}$$

Equation (2.17a) requires that

$$\theta(0, q+1) = 1 \tag{B 3}$$

and (2.17b) requires V to be updated by

$$4SV(q+1) = 1 + \frac{1}{2h}\left[\frac{-11}{3} + 6\theta(1,q) - 3\theta(2,q) + \frac{2}{3}\theta(3,q)\right]. \tag{B 4}$$

Possibly the simplest way of incorporating (2.18) is to require

$$\theta(P, q) = 0 \quad \text{for all} \quad q. \tag{B 5}$$

The integration can then be started by using the power-series representations (A 2) and (A 5) at a suitable value of q.

B.2. *Convergence*

A q-independent solution of (B 1)–(B 5), which reflects the time-independent solution (2.20) and (2.21), satisfies

$$\left(\frac{1}{4}\frac{k}{h^2} + \frac{1}{2}\frac{kV}{h}\right)\theta_{p+1} - \frac{1}{2}\frac{k}{h^2}\theta_p + \left(\frac{1}{4}\frac{k}{h^2} - \frac{1}{2}\frac{kV}{h}\right)\theta_{p-1} = 0, \tag{B 6}$$

where we have written θ_p for $\theta(p, q)$ and V is the constant, steady-state value of $\dot{\eta}$. The solution of (B 6) which satisfies (B 3) is

$$\theta_p = (1+K)\left(\frac{1-2hV}{1+2hV}\right)^p - K, \tag{B 7}$$

where K is a constant. Ideally, $K = 0$ so that $\theta_p \to 0$ as $p \to \infty$. However, (B 5) requires

$$K = \frac{\left(\frac{1-2hV}{1+2hV}\right)^P}{1-\left(\frac{1-2hV}{1+2hV}\right)^P}. \tag{B 8}$$

Since $2hV \ll 1$,

$$K \approx \frac{(1-4hV)^P}{1-(1-4hV)^P}. \tag{B 9}$$

Thus $K \ll 1$ if $4hVP \gg 1$.

It would seem reasonable to think that convergence could be accelerated by altering (B 5) to either

$$\theta(P,q) = \left(\frac{1-2hV(q)}{1+2hV(q)}\right)^P \quad \text{or} \quad \theta(P,q) = \left(\frac{1-2hV}{1+2hV}\right)^P, \tag{B 10a, b}$$

thereby ensuring that $K = 0$ in the steady state. Trial calculations using both procedures were conducted. Neither alteration was useful. In the first, $V(q)$ is quite small for small q and so a value of θ close to 1 was imposed at large P. In the second, the final value of θ at P was imposed too quickly and the solution for low values of q did not agree well with those obtained by using the correct condition (B 5).

Finally, setting $K = 0$ in (B 7) and substituting the results into (B 4), we obtain

$$V = \frac{1}{4(1+S)}[1+O(h^2)], \tag{B 11}$$

in agreement with (2.21).

B.3. *Stability*

Equation (2.16) and its numerical equivalent (B 1) is nonlinear through the product of V and θ. This makes analysis of the stability of the numerical scheme difficult, though some results have been obtained by Griffiths (1982). Some insight can be obtained by setting $V(q)$ to a constant, say $\mathscr{V}$. Because the numerical solutions plotted in figures 3, 8, 12, 15 and 17 indicate that $\dot{\eta}$, or $\mathscr{V}$, becomes constant after some time and the next Appendix proves this is so in the limit $\tau \to \infty$, the results obtained by holding V constant are of definite interest and applicability. Analyses for this case are discussed in Mitchell & Griffiths (1980) and Griffiths, Christie & Mitchell (1980).

Appendix C. The solution for $\tau \gg 1$

The solution for large τ can be obtained by first expressing the solution of (2.8)–(2.11) in an integral representation. Using the embedding technique (Crank 1984) and the integral representation derived in Carslaw & Jaeger (1959, p. 62) for conduction in a semi-infinite solid under a prescribed surface temperature, we can write the solution of (2.8), (2.10) and (2.11) as

$$\theta(\xi,\tau) = \frac{\xi}{\pi^{\frac{1}{2}}}\int_0^\tau \phi(\tau-w)\, w^{-\frac{3}{2}} \exp(-\xi^2/w)\, \mathrm{d}w, \tag{C 1}$$

where

$$\phi(\tau) = \theta(0,\tau). \tag{C 2}$$

Inserting (C 1) into (2.9*a*, *b*), we obtain

$$4S\dot{\eta} = 1+\frac{1}{\pi^{\frac{1}{2}}}\int_0^\tau \phi(\tau-w)\, w^{-\frac{5}{2}}[w-2\eta^2(\tau)]\exp[-\eta^2(\tau)/w]\,\mathrm{d}w \tag{C 3}$$

subject to
$$\eta(\tau)\int_0^\tau \phi(\tau-w)\, w^{-\frac{3}{2}}\exp[-\eta^2(\tau)/w]\,\mathrm{d}w = \pi^{\frac{1}{2}}. \tag{C 4}$$

For $\tau \gg 1$, $\eta(\tau)$ becomes large and we would anticipate that the integrals in (C 3) and (C 4) can be approximated by using standard techniques for the asymptotic evaluation of integrals containing rapidly varying functions (see Murray 1974 and references therein). The dominant contribution in the limit of $\tau \to \infty$ could come from the neighbourhood of either (i) $w = 0$; (ii) $w = \tau$; (iii) some point between 0 and τ; (iv) a combination of these, though this is generically unlikely; or (v) almost equally from the whole range $[0, \tau]$. The initial conditions play a role only if $\phi(0)$ appears in the results, that is only if there is a contribution in the limit of $\tau \to \infty$ from the neighbourhood of $w = \tau$.

(i) Under the assumption that only the neighbourhood of $w = 0$ contributes to (C 4), it can be written as

$$\pi^{-\frac{1}{2}}\eta(\tau)\,\phi(\tau)\int_0^\tau w^{-\frac{3}{2}}\exp[-\eta^2(\tau)/w]\,\mathrm{d}w \sim 1 \tag{C 5a}$$

$$= \phi(\tau)\,\mathrm{erfc}\,[\eta(\tau)/\tau^{\frac{1}{2}}] \tag{C 5b}$$

$$\sim \frac{\tau^{\frac{1}{2}}}{\pi^{\frac{1}{2}}}\frac{\phi(\tau)}{\eta(\tau)}\exp[-\eta^2(\tau)/\tau] \quad (\tau\to\infty), \tag{C 5c}$$

where (C 5*b*) follows from the left-hand side of (C 5*a*) by the integral definition of $\mathrm{erfc}\,(x)$, and (C 5*c*) is the asymptotic expansion of (C 5*b*) on the assumption that $\eta(\tau)/\tau^{\frac{1}{2}} \to \infty$ as $\tau \to \infty$. Similarly, (C 3) can be written

$$4S\dot{\eta} \sim 1+\pi^{-\frac{1}{2}}\phi(\tau)\int_0^\tau w^{-\frac{5}{2}}[w-2\eta^2(\tau)]\exp[-\eta^2(\tau)/w]\,\mathrm{d}w \tag{C 6a}$$

$$= 1-\frac{2\phi(\tau)}{(\pi\tau)^{\frac{1}{2}}}\exp[-\eta^2(\tau)/\tau] \tag{C 6b}$$

$$\sim 1-2\eta(\tau)/\tau \quad (\tau\to\infty), \tag{C 6c}$$

where (C 6*c*), which follows from (C 6*b*) upon substitution of (C 5*c*), has solution

$$\eta(\tau) = \frac{\tau}{4S+2}+C\tau^{-1/(2S)} \tag{C 7a}$$

$$\to \frac{\tau}{4(S+\frac{1}{2})} \quad (\tau\to\infty), \tag{C 7b}$$

where C is an arbitrary constant of integration.

While (C 7*b*) is tantalizingly close to (2.21), it is neither close enough nor correct. Equations (C 5) and (C 7*b*) imply

$$\phi(\tau) \sim \frac{\pi^{\frac{1}{2}}}{4S+2}\tau^{\frac{1}{2}}\exp[-\tau/(4S+2)^2]. \tag{C 8}$$

The insertion of (C 7*b*) and (C 8) into (C 4) leads to the integrand

$$(\tau-w)^{\frac{1}{2}}w^{-\frac{3}{2}}\exp[(w-\tau-\tau^2w^{-1})/(4S+2)^2],$$

the exponential part of which is an *increasing* function of w. This is inconsistent with the original assumption that the dominant contribution comes from the neighbourhood of $w=0$.

(ii) A similar analysis proves that the dominant contribution cannot come from $w=\tau$.

(iii) If the dominant contribution to (C 3) and (C 4) comes from an interior point, the position of the interior point and the form of the contribution will depend critically on the nature of $\phi(\tau)$. I hence think it not possible to analyse the situation without assuming some part of the answer at the outset. A consistency proof seems the best one can obtain.

In this spirit, we note that (2.21) indicates that

$$\eta\rightarrow\tfrac{1}{4}\tau/(1+S)\quad(\tau\rightarrow\infty), \tag{C 9}$$

which when inserted into (2.15) and (2.20) suggests that

$$\phi(\tau)\equiv\theta(0,\theta)\rightarrow\exp[\tfrac{1}{4}\tau/(1+S)^2]. \tag{C 10a, b}$$

Thus
$$\phi(\tau-w)\exp[-\eta^2(\tau)/w]\rightarrow\exp\{-\tfrac{1}{4}(w-\tfrac{1}{2}\tau)^2/[w(1+S)^2]\}. \tag{C 11}$$

The integrands in (C 3) and (C 4) are hence exponentially largest at the interior point $w=\frac{1}{2}\tau$. The left-hand side of (C 4) can thus be written as

$$\eta(\tau)\int_0^\tau w^{-\frac{3}{2}}\exp\{-\tfrac{1}{4}(w-\tfrac{1}{2}\tau)^2/[w(1+S)^2]\}\,\mathrm{d}w$$

$$\sim\eta(\tau)(\tfrac{1}{2}\tau)^{-\frac{3}{2}}\int_{-\infty}^{\infty}\exp\{-\tfrac{1}{2}u^2/[\tau(1+S)^2]\}\,\mathrm{d}u \tag{C 12}$$

$$=4\pi^{\frac{1}{2}}(1+S)\,\eta(\tau)/\tau. \tag{C 13}$$

Inserting (C 13) into (C 4), we obtain (C 9), as required. In a similar fashion (C 3) can be shown to be satisfied by (C 9) and (C 10). This also indicates that the possibilities (iv) and (v) outlined above do not occur. Finally, it is worth remarking that it is *not* possible to use (C 3) and (C 4) to solve the problem for all $\tau>0$. This is because the integral representation (C 1) is only valid for $\xi>0$, though this is not stated, or needed, by Carslaw & Jaeger (1959).

Appendix D. The initial solution for $T_m<T_i$ with $\tau_0=0$

A representation as a power series in $\tau^{\frac{1}{2}}$ for the solution of (2.10), (2.11), (5.2)–(5.4) can be obtained by using the concepts, rather than the formality, of the embedding technique. This suggests that the solution will be of the form

$$\theta(\xi,\tau)=\sum_{n=0}^{\infty}\tau^{\frac{1}{2}n}[B_n\,i^n\operatorname{erfc}(\xi/\tau^{\frac{1}{2}})+C_n\,i^n\operatorname{erfc}(-\xi/\tau^{\frac{1}{2}})]\quad[\eta_U(\tau)<\xi<\eta_L(\tau)] \tag{D 1}$$

$$=\sum_{n=0}^{\infty}\tau^{\frac{1}{2}n}D_n\,i^n\operatorname{erfc}(\xi/\tau^{\frac{1}{2}})\quad[\eta_L(\tau)<\xi], \tag{D 2}$$

where the B_n, C_n and D_n are determined from

$$\sum_{n=0}^{\infty} \tau^{\frac{1}{2}n}[B_n\, i^n \operatorname{erfc}(\eta_U/\tau^{\frac{1}{2}}) + C_n\, i^n \operatorname{erfc}(-\eta_U/\tau^{\frac{1}{2}})] = 1, \tag{D 3}$$

$$\sum_{n=0}^{\infty} \tau^{\frac{1}{2}(n-1)}[B_n\, i^{n-1} \operatorname{erfc}(\eta_U/\tau^{\frac{1}{2}}) - C_n\, i^{n-1} \operatorname{erfc}(-\eta_U/\tau^{\frac{1}{2}})] = 1 - 4S\dot{\eta}_U, \tag{D 4}$$

$$\sum_{n=0}^{\infty} \tau^{\frac{1}{2}n}[B_n\, i^n \operatorname{erfc}(\eta_L/\tau^{\frac{1}{2}}) + C_n\, i^n \operatorname{erfc}(-\eta_L/\tau^{\frac{1}{2}})] = \delta, \tag{D 5}$$

$$\sum_{n=0}^{\infty} \tau^{\frac{1}{2}n} D_n\, i^n \operatorname{erfc}(\eta_L/\tau^{\frac{1}{2}}) = \delta, \tag{D 6}$$

$$\sum_{n=0}^{\infty} \tau^{\frac{1}{2}(n-1)}[D_n\, i^{n-1} \operatorname{erfc}(\eta_L/\tau^{\frac{1}{2}}) - B_n\, i^{n-1} \operatorname{erfc}(-\eta_L/\tau^{\frac{1}{2}})] + C_n\, i^{n-1} \operatorname{erfc}(-\eta_L/\tau^{\frac{1}{2}})] = -4S\dot{\eta}_L. \tag{D 7}$$

Inserting the expansions

$$\eta_U(\tau) = \sum_{n=1}^{\infty} p_{n-1}\tau^{\frac{1}{2}n} \quad \text{and} \quad \eta_L(\tau) = \sum_{n=1}^{\infty} q_{n-1}\tau^{\frac{1}{2}n} \tag{D 8a, b}$$

into (D 3)–(D 7) and equating like powers of τ, we can obtain systems of equations for the unknown expansion coefficients. The lowest-order system is nonlinear and given by

$$E_0 \operatorname{erfc} p_0 + 2C_0 = 1, \quad E_0 + \pi^{\frac{1}{2}} S p_0 \exp(p_0^2) = 0, \tag{D 9a, b}$$

$$E_0 \operatorname{erfc} q_0 + 2C_0 = \delta, \tag{D 9c}$$

$$D_0 \operatorname{erfc} q_0 = \delta, \quad D_0 - E_0 + \pi^{\frac{1}{2}} S q_0 \exp(q_0^2) = 0, \tag{D 9d, e}$$

where

$$E_0 = B_0 - C_0. \tag{D 10}$$

Equations (D 9) must be solved numerically. All the higher-order systems are linear and the next one is given by

$$B_1 \operatorname{ierfc} p_0 + C_1 \operatorname{ierfc}(-p_0) - 2\pi^{-\frac{1}{2}} E_0 \exp(-p_0^2)\, p_1 = 0, \tag{D 11a}$$

$$B_1 \operatorname{erfc} p_0 - C_1 \operatorname{erfc}(-p_0) + 4S(1+p_0^2)\, p_1 = 1, \tag{D 11b}$$

$$B_1 \operatorname{ierfc} q_0 + C_1 \operatorname{ierfc}(-q_0) - 2\pi^{-\frac{1}{2}} E_0 \exp(-q_0^2)\, q_1 = 0, \tag{D 11c}$$

$$D_1 \operatorname{ierfc} q_0 - 2\pi^{-\frac{1}{2}} D_0 \exp(-q_0^2)\, q_1 = 0, \tag{D 11d}$$

$$D_1 \operatorname{erfc} q_0 - B_1 \operatorname{erfc} q_0 + C_1 \operatorname{erfc}(-q_0) + 4S(1+q_0^2)\, q_1 = 0. \tag{D 11e}$$

Solutions to (D 9) and (D 11) were used as initial inputs to the numerical integrations.

In the limit of large S, (D 9) and (D 11) can be shown to be satisfied by

$$-p_0 = q_0 = \tfrac{1}{2}(1-\delta)^{\frac{1}{2}} S^{-\frac{1}{2}}[1 + O(S^{-\frac{1}{2}})] \tag{D 12a, b}$$

and

$$p_1 = 5q_1 = \tfrac{5}{24} S^{-1} \quad [1 + O(S^{-\frac{1}{2}})]. \tag{D 13a, b}$$

REFERENCES

ABRAMOVITZ, M. & STEGUN, I. A. 1964 *Handbook of Mathematical Functions.* US Government Printing Office.

BRUCE, P. M. 1989 Convective heat transfer within the Earth's crust. Ph.D. dissertation, Cambridge University.

CARSLAW, H. S. & JAEGER, J. C. 1959 *Conduction of Heat in Solids.* Oxford University Press.

CLAOUÉ-LONG, J. C. & NESBITT, R. W. 1985 Contaminated komatiites. *Nature* **313**, 247.

CRANK, J. 1984 *Free and Moving Boundary Problems.* Oxford University Press.

CROWLEY, A. B. & OCKENDON, J. R. 1977 A Stefan problem with a non-monotone boundary. *J. Inst. Maths Applics* **20**, 269–281.

GRIFFITHS, D. F. 1982 The stability of finite difference approximations to non-linear partial differential equations. *Bull. Inst. Maths Applics* **18**, 210–215.

GRIFFITHS, D. F., CHRISTIE, I. & MITCHELL, A. R. 1980 Analysis of error growth for explicit difference schemes in conduction–convection problems. *Intl J. Num. Meth. Engng* **15**, 1075–1081.

HILL, J. M. 1987 *One-dimensional Stefan Problems: An Introduction.* Longman.

HOLMAN, J. P. 1976 *Heat Transfer.* McGraw-Hill.

HUPPERT, H. E. 1986 The intrusion of fluid mechanics into geology. *J. Fluid Mech.* **173**, 557–594.

HUPPERT, H. E. & SPARKS, R. S. J. 1985 Komatiites I: Eruption and flow. *J. Petrol.* **26**, 694–725.

HUPPERT, H. E. & SPARKS, R. S. J. 1988 Melting the roof of a chamber containing a hot, turbulently convecting fluid. *J. Fluid Mech.* **188**, 107–131.

HUPPERT, H. E., SPARKS, R. S. J., TURNER, J. S. & ARNDT, N. T. 1984 Emplacement and cooling of komatiite lavas. *Nature* **309**, 19–22.

LANDAU, H. G. 1950 Heat conduction in a melting solid. *Q. Appl. Maths* **8**, 81–94.

MITCHELL, A. R. & GRIFFITHS, D. F. 1980 *The Finite Difference Method in Partial Differential Equations.* Wiley.

MURRAY, J. D. 1974 *Asymptotic Analysis.* Springer.

SAVINO, J. M. & SIEGEL, R. 1969 An analytical solution for solidification of a moving warm liquid onto an isothermal cold wall. *Intl J. Heat Mass Transfer* **12**, 803–809.

SMITH, G. D. 1965 *Numerical Solution of Partial Differential Equations.* Oxford University Press.

TAO, L. N. 1978 The Stefan problem with arbitrary initial and boundary conditions. *Q. Appl. Maths* **36**, 223–233.

TARZIA, D. A. 1988 *Bibliography on Moving Free Boundary Problems for the Heat-Diffusion Equation. The Stefan Problem.* Instituto Matematico "Ulisee Dini", Florence.

TURNER, J. S. 1973 *Buoyancy Effects in Fluids.* Cambridge University Press.